



1 **Global assessment of how averaging over land-surface heterogeneity affects modeled evapotranspiration rates**

2

3 Elham Rouholahnejad Freund^{1,2}, Ying Fan³, James W. Kirchner^{2,4,5}

4

5 ¹Laboratory of Hydrology and Water Management, Ghent University, Ghent, Belgium

6 ²Department of Environmental Systems Science, ETH Zurich, 8092, Zurich, Switzerland

7 ³Department of Earth and Planetary Sciences, Rutgers University, New Brunswick, NJ, United States

8 ⁴Swiss Federal Research Institute WSL, Birmensdorf, 8903, Switzerland

9 ⁵Dept. of Earth and Planetary Science, University of California, Berkeley, CA 94720, United States

10

11 *Correspondence to:* Elham Rouholahnejad Freund, elham.rouholahnejad@gmail.com

12

13 **Key points**

14 - Evapotranspiration rates and the properties that regulate them are spatially heterogeneous at scales
15 orders of magnitude smaller than typical Earth System Models (ESMs) grid cells. Averaging over this spatial
16 heterogeneity may lead to biased estimates of energy and water fluxes in ESMs.

17 - We quantified the effects of averaging over spatial heterogeneity on grid-cell-averaged evapotranspiration
18 (ET) rates over heterogeneous landscapes across the globe and highlighted the locations where the
19 heterogeneity bias matters. We showed that because the relationships driving ET are nonlinear, averaging
20 over sub-grid heterogeneity of drivers of ET, namely precipitation (P) and potential evapotranspiration
21 (PET), leads to overestimation of average ET.

22 - Our analysis showed that this "heterogeneity bias" is most pronounced in mountainous terrain, in
23 landscapes where P is inversely correlated with PET, and in regions with temperate climates and dry
24 summers.

25 - We showed that the magnitude of this heterogeneity bias grows on average, and expands over larger
26 areas, as the size of the grid cell increases.

27



28 **Abstract**

29 The major goal of large-scale Earth System Models (ESMs) is to understand and predict global change. However,
30 computational constraints require ESMs to operate on relatively large spatial grids (typically \sim 1 degree or \sim 100 km
31 in size) with the result that the heterogeneity in land surface properties and processes at smaller spatial scales
32 cannot be explicitly represented. Averaging over this spatial heterogeneity may lead to biased estimates of energy
33 and water fluxes in ESMs. For example, evapotranspiration rates and the properties that regulate them are spatially
34 heterogeneous at scales orders of magnitude smaller than typical ESM grid cells. Here we quantify the effects of
35 spatial heterogeneity on grid-cell-averaged evapotranspiration (ET) rates, as seen from the atmosphere over
36 heterogeneous landscapes across the globe. In an earlier study, we used a Budyko framework to functionally relate
37 ET to precipitation (P) and potential evapotranspiration (PET), and used a sub-grid closure relation to quantify the
38 effects of sub-grid heterogeneity on average ET at 1° by 1° grid cells- the scale of typical ESM. We showed that
39 because the relationships driving ET are nonlinear, averaging over sub-grid heterogeneity in P and PET leads to
40 overestimation of average ET. In this study, we extend that work to the globe and examine the global distribution of
41 this bias, its scale dependence, and the underlying mechanisms. Our analysis shows that this "heterogeneity bias" is
42 more pronounced in mountainous terrain, in landscapes where P is inversely correlated with PET, and in regions
43 with temperate climates and dry summers. We also show that the magnitude of this heterogeneity bias grows on
44 average, and expands over larger areas, as the size of the grid cell increases. Correcting for this overestimation of
45 ET in ESMs is important for modeling the water cycle, as well as for future temperature predictions, since current
46 overestimations of ET rates imply smaller sensible heat fluxes, and potential underestimation of dry and warm
47 conditions in the context of climate change. Our work provides a basis for translating the heterogeneity bias into
48 correction factors in large-scale ESMs, and highlights the regions where more detailed mechanistic modeling is
49 needed.

50

51



52 **1. Introduction**

53 Earth System Models (ESMs) are designed to understand interactions between the land surface, atmosphere, and
54 oceans and to predict global environmental changes. However, the Earth system and its underlying physical
55 processes are highly heterogeneous across orders of magnitude in scale below the scale of typical ESM grids (e.g.,
56 1° by 1°). Despite increasing recognition of the need to mechanistically represent physical processes in ESMs,
57 currently even the most disaggregated large-scale ESMs cannot explicitly represent the spatial heterogeneity of
58 land surface hydrological properties at scales that are important to atmospheric fluxes. Overlooking this spatial
59 heterogeneity and instead averaging over land surface properties at the scale of ESM model grid cells may have
60 important implications for water and energy flux estimates in large-scale ESMs (Avissar and Pielke, 1989; Giorgi and
61 Avissar, 1997; Ershadi et al., 2013; Lu et al., 2014).

62

63 Estimates of evapotranspiration (ET) fluxes have significant implications for future temperature predictions. Smaller
64 ET fluxes imply greater sensible heat fluxes and therefore, amplified dry and warm conditions in the context of
65 climate change (Seneviratne et al., 2010). Surface evaporative fluxes (and thus energy partitioning over land
66 surfaces) are nonlinear functions of available water and energy, and thus are coupled to spatially heterogeneous
67 surface characteristics (e.g., soil type, vegetation, topography) and meteorological inputs (e.g., radiative flux, wind,
68 and precipitation) (Kalma et al., 2008; Shahraeeni and Or, 2010; Holland et al., 2013). These characteristics are
69 spatially variable on length scales of <1 m to many kilometers, well below typical ESM grid scales of ~100 km. ESMs
70 calculate grid-averaged surface and atmospheric fluxes from grid-averaged land surface parameterizations (Sato et
71 al., 1989; Koster et al., 2006; Santanello and Peters-Lidard, 2011). Thus ET estimates that are derived from spatially-
72 averaged land surface properties do not capture ET variations driven by the underlying surface heterogeneity
73 (McCabe and Wood, 2006). Because the relationships driving ET are nonlinear, the average ET flux from a
74 heterogeneous landscape may be different from an ET estimate calculated from spatially averaged inputs
75 (Rouholahnejad Freund and Kirchner, 2017).

76

77 Several studies have quantified the effects of land surface heterogeneity on ET, potential evapotranspiration (PET),
78 and latent heat (LH) fluxes, and have found that averaging over land surface heterogeneity can potentially bias ET
79 estimates either positively or negatively. For example, Boone and Wetzel (1998) studied the effects of soil texture
80 variability within each pixel in the Land-Atmosphere-Cloud Exchange (PLACE) model, which has a spatial resolution
81 of approximately 100 by 100 km. They reported that accounting for sub-grid variability in soil texture reduced
82 global ET by 17%, increased total runoff by 48%, and increased soil wetness by 19%, compared to using a
83 homogenous soil texture to describe the entire grid cell. Kollet (2009) found that heterogeneity in soil hydraulic
84 conductivity had a strong influence on evapotranspiration during the dry months of the year, but not during
85 months with sufficient moisture availability. Hong et al. (2009) reported that aggregating radiance data from 30 m
86 to 60, 120, 250, 500, and 1000 m resolution (input upscaling) and then calculating ET from these aggregated inputs
87 at these grid scales using Surface Energy Balance Algorithm for Land (SEBAL, Bastiaanssen et al., 1998a) yields



88 slightly larger ET estimates as compared to ET calculated with finer resolution inputs and then aggregated at the
89 desired grid scales (output upscaling). The discrepancy between ET estimated with the output upscaling method
90 and the input upscaling method grows as the size of the grid-cell increases (the difference between ET calculated
91 from the input and output upscaling methods is ~20% more at a grid scale of 1 km by 1 km compared to grid scale
92 of 120 m by 120 m). Aminzadeh et al. (2017) investigated the effects of averaging surface heterogeneity and soil
93 moisture availability on potential evaporation from a heterogeneous land surface including bare soil and vegetation
94 patches. They found that if the heterogeneity length scale is smaller than the convective atmospheric boundary
95 layer (ABL) thickness, averaging over heterogeneous land surfaces has only a small effect on average potential
96 evaporation rates. Averaging over larger-scale heterogeneities, however, led to overestimates of potential
97 evaporation.

98

99 McCabe and Wood (2006) found that remote sensing retrievals of ET are larger than the corresponding in-situ flux
100 estimates and characterized the roles of land surface heterogeneity and remote sensing resolution in the retrieval
101 of evaporative flux. McCabe and Wood (2006) used Landsat (60 m), Advanced Space borne Thermal Emission and
102 Reflection Radiometer (ASTER) (90 m), and MODIS (1020 m) independently to estimate ET over the Walnut Creek
103 watershed in Iowa. They compared these remote sensing estimates to eddy covariance flux measurements and
104 reported that Landsat and ASTER ET estimates had a higher degree of consistency with one another and correlated
105 better to the ground measurements (0.87 and 0.81, respectively) than MODIS- based ET estimates did. All three
106 remote sensing products overestimated ET as compared to ground measurements (at 12 out of 14 tower sites).
107 Upon aggregation of Landsat and ASTER retrievals to MODIS scale (1 km), the correlation with the ground
108 measurements decreased to 0.75 and 0.63 for Landsat and ASTER, respectively.

109

110 Contrary to overestimation bias, many remotely sensed ET estimates that include parameters related to
111 aerodynamic resistance are significantly affected by heterogeneity, and underestimate ET as the scale increases
112 (Ershadi et al., 2013). Because aerodynamic resistance is significantly affected by land surface properties (e.g.,
113 vegetation height, roughness length, and displacement height), decreases in aerodynamic resistance at coarser
114 resolutions could lead to smaller estimates of evapotranspiration. Ershadi et al. (2013) showed that input
115 aggregation from 120m to 960 m in Surface Energy Balance System (SEBS, Su, 2002) leads to up to 15 %
116 underestimation of ET at the aggregated grid resolution in a study area in the south-east of Australia.

117 Rouholahnejad Freund and Kirchner (2017) quantified the impact of sub-grid heterogeneity on grid-average ET
118 using a simple Budyko curve (Turc, 1954; Mezentsev, 1955) in which long-term average ET is a non-linear function
119 of long-term averages of precipitation (P) and potential evaporation (PET). They showed mathematically that
120 averaging over spatially heterogeneous P and PET results in overestimation of ET (Fig. 1). Their analysis implies that
121 large-scale ESMs that overlook land surface heterogeneity will yield biased evapotranspiration estimates due to the
122 inherent nonlinearity in ET processes. They did not, however, estimate the likely magnitude of this heterogeneity
123 bias beyond a few example grid cells.



124

125 The recognition that spatial averaging can potentially lead to biased flux estimates has prompted methods for
126 representing sub-grid-scale heterogeneities and processes within ESMs. Accounting for land surface heterogeneity
127 in large-scale ESMs is constrained by limitations in both computational power (Baker et al. 2017) and the availability
128 of high-resolution forcing data. There have been several attempts to integrate sub-grid heterogeneity in ESMs while
129 maintaining the computational costs affordable. In “mosaic” approaches, the model is run separately for each
130 surface type in a grid cell, and then the surface specific fluxes are area-weighted to calculate the grid-cell average
131 fluxes (e.g., Avissar and Pielke, 1989; Koster and Suarez, 1992). The “effective parameter” approach (e.g., Wood
132 and Mason, 1991; Mahrt et al., 1992), by contrast, seeks to estimate effective parameter values at the grid cell
133 scale that subsume the effects of sub-grid heterogeneity. Estimating these effective parameters can be challenging
134 because the relevant land-surface processes typically depend nonlinearly on multiple interacting parameters, and
135 land-surface signals at different scales are propagated and diffused differently in the atmosphere. Alternatively, the
136 “correction factor” approach (e.g., Maayar and Chen, 2006) uses sub-grid information on spatially heterogeneous
137 land-surface processes and properties to estimate multiplicative correction factors for fluxes that are originally
138 calculated from spatially averaged inputs at the grid-cell scale. All three approaches try to reduce the
139 heterogeneous problem to a homogeneous one that has equivalent effects on the atmosphere at the grid-cell
140 scale.

141

142 There is a growing need to understand how sub-grid heterogeneity and the atmosphere’s integration of it, affect
143 grid-scale water and energy fluxes, and to develop effective methods to incorporate these effects in ESMs (Clark et
144 al., 2015, Fan et al., 2019). The above-mentioned studies present the potential effects of spatial heterogeneity on
145 water and energy flux estimates in land surface models at several scales, but are deficient in proposing a general
146 framework for quantifying systematic biases in ET estimates due to averaging over heterogeneities. In a previous
147 study, we used the Budyko framework as a simple estimator of ET, and demonstrated theoretically how averaging
148 over heterogeneous precipitation and potential evapotranspiration at the grid scale of a typical ESM (e.g., 1° by 1°)
149 can lead to systematic overestimation of long-term average ET fluxes from heterogeneous landscapes. In the
150 present study, we apply that analysis across the globe and highlight the locations where the heterogeneity bias
151 matters. Our hypotheses are that, (1) strongly heterogeneous landscapes, such as mountainous terrain, will exhibit
152 higher bias due to averaging, (2) the bias will be higher in climates where P and PET are inversely correlated in
153 space, and (3) heterogeneity bias will decrease as the spatial scales of averaging decrease.

154

155 **2. Effects of sub-grid heterogeneity on ET estimates in the Budyko framework**

156 Budyko (1974) showed that the long-term annual average evapotranspiration is a function of both the supply of
157 water (precipitation, P) and the evaporative demand (potential evapotranspiration, PET) under steady-state
158 conditions and in catchments with negligible changes in storage (Eq. 1; Turc, 1954; Mezentsev, 1955).



159

$$ET = f(P, PET) = \frac{P}{\left(\left(\frac{P}{PET}\right)^n + 1\right)^{1/n}}. \quad (1)$$

160 Evapotranspiration rates are inherently bounded by energy and water limits. Under arid conditions ET is limited by
 161 the available supply of water (the water limit line in Fig. 1b), while under humid conditions ET is limited by
 162 atmospheric demand (PET) and converges toward PET (the energy limit line in Fig. 1b). Budyko showed that over a
 163 long period and under steady-state conditions, hydrological systems function close to their energy or water limits.
 164 These intrinsic water and energy constraints make the Budyko curve downward-curving.

165

166 In a heterogeneous landscape, like the simple example of two ESM columns in Fig. 1a, P and PET vary spatially. The
 167 two columns with heterogeneous P and PET are represented by the two solid black circles on the Budyko curve in
 168 Fig. 1b. In this hypothetical two-column example, the true average of ET values calculated from individual
 169 heterogeneous inputs (the solid black circles) lies below the curve (the grey circle, labeled "true average").
 170 However, if we aggregate the two columns and consider the system as one column with average properties, the
 171 function of average inputs (averaged P and PET over the two columns) lies on the Budyko curve (the open circle)
 172 which is larger than the true average of the two columns. In short, in any downward curving function, the function
 173 of the average inputs (the open circle) will always be larger than the average of the individual function values (the
 174 true average; grey circle). The difference between the two can be termed the "heterogeneity bias".
 175 Rouholahnejad Freund and Kirchner (2017) showed that when nonlinear underlying relationships are used to
 176 predict average behaviour from averaged properties, the magnitude of the resulting heterogeneity bias can be
 177 estimated from the degree of the curvature in the underlying function and the range spanned by the individual data
 178 being averaged. The second-order, second-moment Taylor expansion of the ET function $f(P, PET)$ (Eq. 1) around its
 179 mean directly yields:

$$180 \bar{f}(P, PET) = \bar{ET} \approx f(\bar{P}, \bar{PET}) + \frac{1}{2} \frac{\partial^2 f}{\partial P^2} var(P) + \frac{1}{2} \frac{\partial^2 f}{\partial PET^2} var(PET) + \frac{\partial^2 f}{\partial P \partial PET} cov(P, PET) , \quad (2)$$

181 where $\bar{f}(P, PET)$ is the true average of the spatially heterogeneous ET function, $f(\bar{P}, \bar{PET})$ is the ET function
 182 evaluated at average inputs \bar{P} and \bar{PET} , and where the derivatives are quantified at \bar{P} and \bar{PET} . Evaluating the
 183 derivatives using Eq. (1) and reshuffling the terms, Rouholahnejad Freund and Kirchner (2017) obtained the
 184 following expression for the heterogeneity bias, the difference between the average ET, $\bar{f}(P, PET)$, and the ET
 185 function evaluated at the mean of its inputs, $f(\bar{P}, \bar{PET})$:

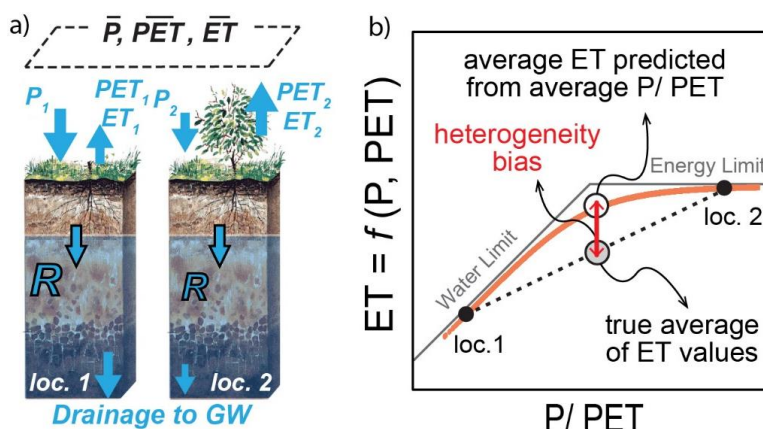
$$186 f(\bar{P}, \bar{PET}) - \bar{f}(P, PET) \approx (n+1) \frac{\bar{P}^{n+1} \bar{PET}^{n+1}}{(\bar{P}^n + \bar{PET}^n)^{2+1/n}} \left[\frac{1}{2} \frac{var(P)}{\bar{P}^2} + \frac{1}{2} \frac{var(PET)}{\bar{PET}^2} - \frac{cov(P, PET)}{\bar{P} \bar{PET}} \right]. \quad (3)$$

187 As shown by Fig. 1b and Eq. (2), the discrepancy between average of the ET function and the ET function of the
 188 average inputs (the heterogeneity bias) is proportional to both the degree of nonlinearity in the function, as
 189 defined by its second derivatives, and the range of variation in its input variables, as defined by their variances. Eq.
 190 (3) allows one to estimate how much the curvature of a nonlinear relationship and the variance of its inputs at any



191 desired scale will affect estimates of the true mean. However, to the best of our knowledge, the consequences of
 192 these nonlinearities for global evaporative flux estimates have not previously been quantified.

193



194

195 Figure 1. Heterogeneity bias in a hypothetical two-column model in the Budyko framework. The true average ET of
 196 the columns (gray circle) lies below the curve and is less than the average ET estimated from the average P/PET of
 197 the two columns (open circle). The heterogeneity bias depends on the curvature of the function and the spread of
 198 its inputs.

199

200 3. Effects of sub-grid heterogeneity on ET estimates at 1° by 1° grid scale across the globe

201 Across a landscape of size similar to a typical ESM grid cell (1° by 1°), soil moisture, atmospheric demand (PET) and
 202 precipitation (P) will vary with topographic position; hillslopes will typically be drier, and riparian regions will be
 203 wetter. To quantify the likely biases introduced by averaging over this land surface heterogeneity, we used the
 204 approach outlined in section 2 to the global land surface area at 1° by 1° grid scale. Within each 1° by 1° grid cell,
 205 we used 30 arc-second values of P (WorldClim; Hijmans et al., 2005) and PET (WorldClim; Hijmans et al., 2005) to
 206 examine the variations in small-scale climatic drivers of ET. Because 30 arc-seconds is nearly 1 km, hereafter we
 207 refer to 30 arc-second data as 1km values for simplicity. The spatial distribution of long-term annual averages
 208 (1960-1990) of P and PET values at 1 km resolution and 1km values of the aridity index (AI=P/PET) are shown in Fig
 209 2a-c. ET estimated from these 1km P and PET values using Eq. 1 are then averaged at 1° by 1° scale (“true average”,
 210 Fig. 2e). To mimic the averaging that takes place within ESMs, we also averaged the 1km values of P and PET within
 211 each grid cell and then modeled ET using Eq. 1 applied to these averaged input values. The difference between
 212 these two ET estimates is the heterogeneity bias.

213

214 We also calculated the heterogeneity bias using Eq. (3), which describes how the nonlinearity in the governing
 215 equation and the heterogeneity in P and PET jointly contribute to the heterogeneity bias. The heterogeneity bias



216 estimates obtained by direct calculation and by Eq. (3) were functionally equivalent ($R^2=0.97$, root mean square
217 error of 0.17%).

218

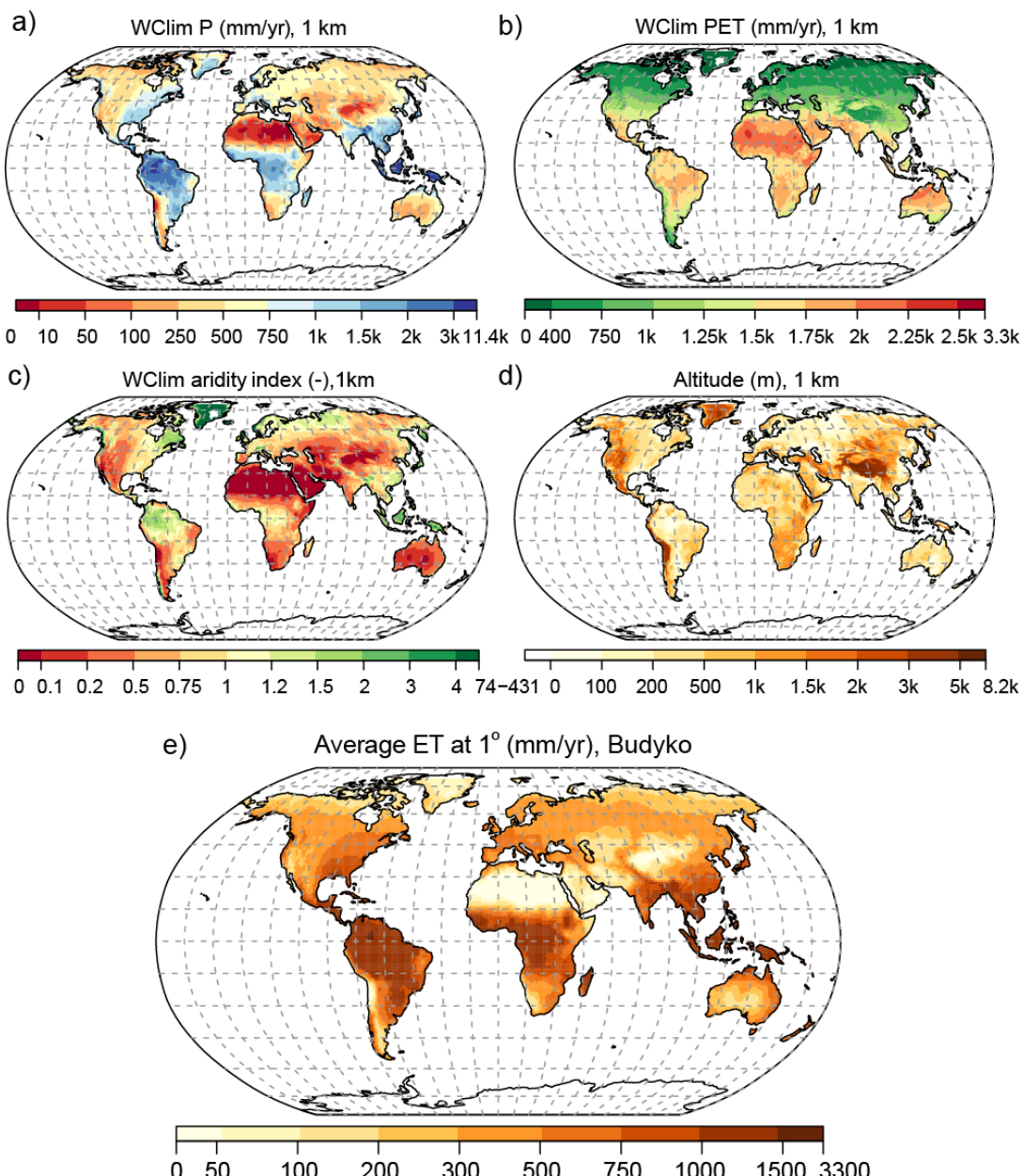
219 Fig. 3a-d illustrates the variability (quantified by standard deviation) of 1km values of P, PET, aridity index, and
220 altitude at the 1° by 1° grid scale. The heterogeneity bias in long-term average ET fluxes at the 1° by 1° grid scale
221 (Fig. 3e) highlights regions around the globe where ET fluxes are likely to be systematically overestimated. The
222 spatial distribution of the heterogeneity bias (Fig. 3e) closely coincides with locations with large variability in the
223 aridity index (Fig. 3c), which is driven in turn by topographic variability (Fig. 3d). Strongly heterogeneous landscapes
224 exhibit significant heterogeneity biases in long-term average ET fluxes, although the global average heterogeneity
225 bias is small (<1%). Physically based ET calculations may exhibit larger heterogeneity biases than the modest values
226 we calculate here, because the Budyko approach already subsumes spatial heterogeneity effects at the catchment
227 scale (and also temporal heterogeneity effects due to its steady- state assumptions). The heterogeneity bias in ET
228 estimates shown in Fig. 3e corresponds to long-term average ET estimates. Given the fact that P and PET can vary
229 temporally (i.e., seasonality), the estimated bias could be much larger, particularly where P and PET are inversely
230 correlated (see the last term of Eq. 3).

231

232 Our results show that the topographic gradient and hence the variability in aridity index across a desired grid size
233 exhibit consistent, predictable patterns of associated prediction bias in evapotranspiration estimates at that scale.
234



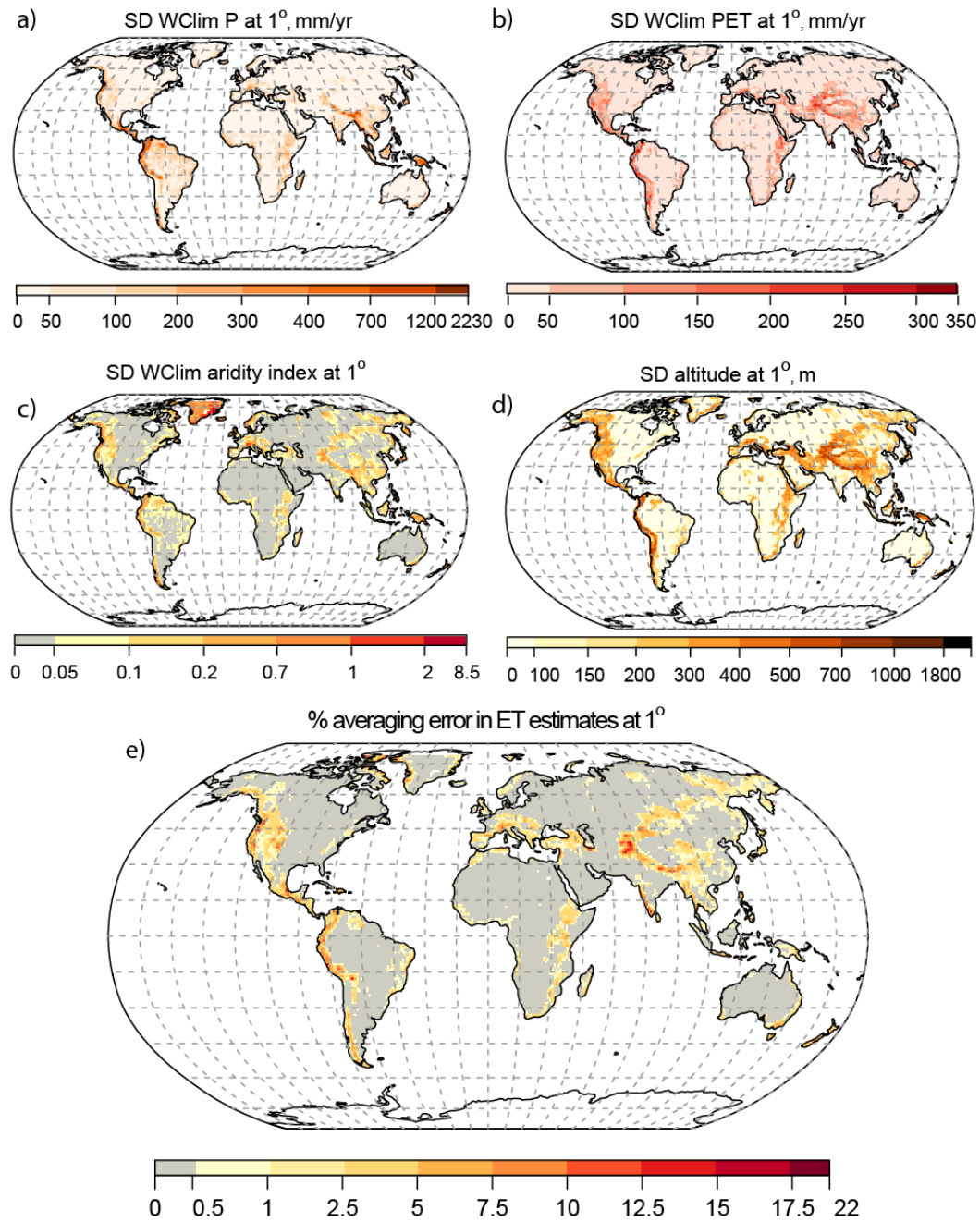
235



236

237 Figure 2. Global distribution of one-kilometer resolution annual mean precipitation (a: P; WorldClim; Hijmans et al.,
238 2005), potential evapotranspiration (b: PET; WorldClim; Hijmans et al., 2005), aridity index (c: AI=P/PET; WorldClim;
239 Hijmans et al., 2005), topography (d: SRTM; Jarvis et al., 2008), and (e) evapotranspiration (ET) at 1° by 1° scale by
240 averaging 1km values of ET calculated using the Budyko function (Eq. 1).

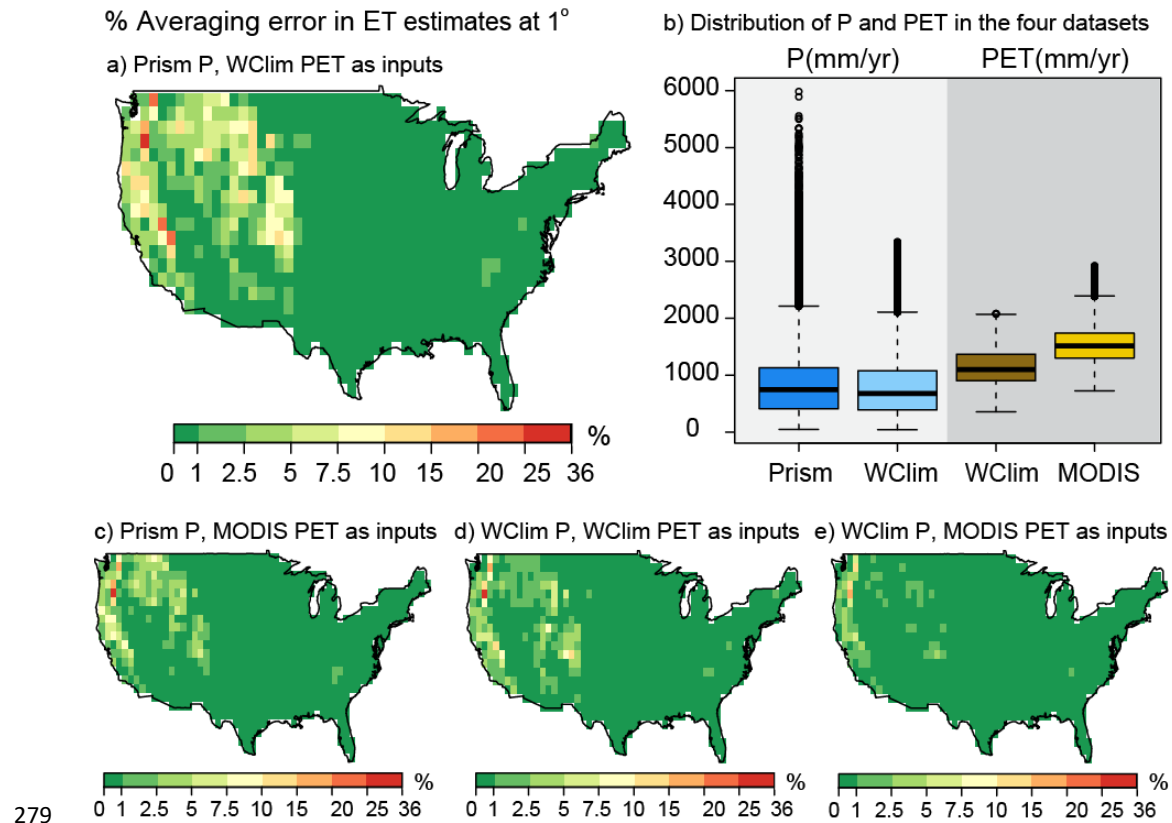
241



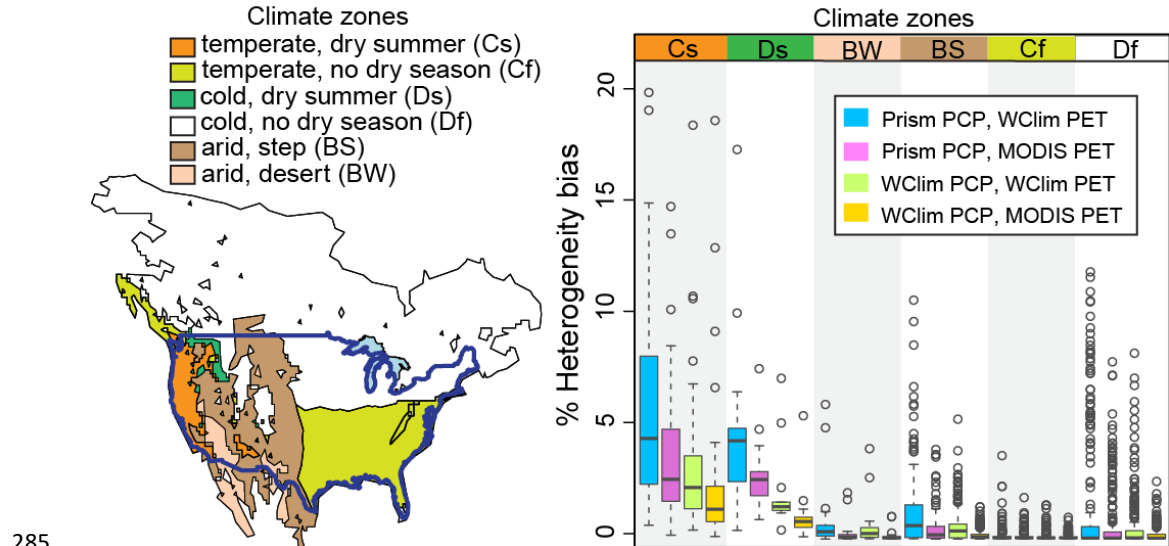
242
243 Figure 3. Global spatial distribution of variability (standard deviation) of one-kilometer values of a) precipitation (P),
244 b) potential evapotranspiration (PET), c) aridity index (AI=P/PET), and d) altitude at 1° by 1° grid cell. The
245 approximated averaging bias in ET estimates (e) is calculated using Eq. (3). Grid cells with large standard deviation
246 in altitude and aridity index encounter higher percentage of averaging bias.



247 **4. Variation in heterogeneity bias across climate zones, data sources, and grid scales**
248 With increased availability of spatial data, it is becoming standard practice to assess input data uncertainties and
249 their propagated impacts on water and energy flux estimates in land surface models. To quantify how choices
250 among alternative input data products could affect the heterogeneity bias in ET estimates, we calculated the
251 heterogeneity bias at 1° by 1° grid cell resolution across the contiguous US using four different pairs of P and PET
252 data products. Two precipitation data sets, Prism (<http://prism.oregonstate.edu>) and WorldClim (Hijmans et al.,
253 2005), along with two PET data sets, MODIS (Mu et al., 2007) and WorldClim (Hijmans et al., 2005), all at 1 km
254 resolution, were combined in all possible pairs. The heterogeneity bias in ET estimates (Eq. 3), as outlined in
255 section 2, was evaluated from 1km values of P, PET, and the estimated average ET using the Budyko relationship
256 (Eq. 1) for each of the four input data pairs. Fig. 4a-e compares the spatial distributions of heterogeneity bias across
257 the contiguous US for the four pairs of P and PET data products. The heterogeneity bias in ET estimates reached as
258 high as 36 % in the western US using Prism P and WorldClim PET as input to the ET model (Fig. 4a). A visual
259 comparison of Figs. 4a, c, d, and e shows that the choice of P data source (Prism vs. WorldClim) had a bigger effect
260 on the heterogeneity bias than the choice of PET data source (MODIS vs. WorldClim). In all cases, data sources that
261 were more variable in relation to their means (Prism for P and WorldClim for PET; Fig. 4b) led to larger
262 heterogeneity biases, as expected from Eq. (3). If we had conducted our global analysis (Fig. 3) with Prism P and
263 either WorldClim or MODIS PET we would have obtained larger heterogeneity biases, but Prism P is not freely
264 available globally.
265
266 If we divide the heterogeneity biases shown in Fig. 4 by Köppen-Geiger climate zones (Peel et al., 2007; Fig. 5), we
267 see that the heterogeneity bias is distinctly higher in particular climate-terrain combinations. The
268 heterogeneity bias is higher in regions with temperate climate and dry summers (climate zone Cs) and in regions
269 with cold, dry summers (climate zone Ds) perhaps due to the sharp spatial gradient in their water and energy
270 sources for evapotranspiration. These areas typically have high topographic relief, combined with seasonal climate.
271 The heterogeneity effects on ET estimates in these regions are expected to be even higher when a mechanistic
272 model of ET is used. We expect that averaging over temporal variations of drivers of ET, especially in places with
273 strong seasonality, could bias the ET estimates but can not be quantified in the Budyko framework due to its
274 underlying steady-state assumptions. Figure 5 also illustrates the relative magnitudes of the heterogeneity biases
275 obtained with the four pairs of P and PET data sources. The heterogeneity bias generally decreases in the order:
276 Prism P-WorldClim PET >> Prism P-MODIS PET >> WorldClim P-WorldClim PET >> WorldClim P-MODIS PET.
277
278



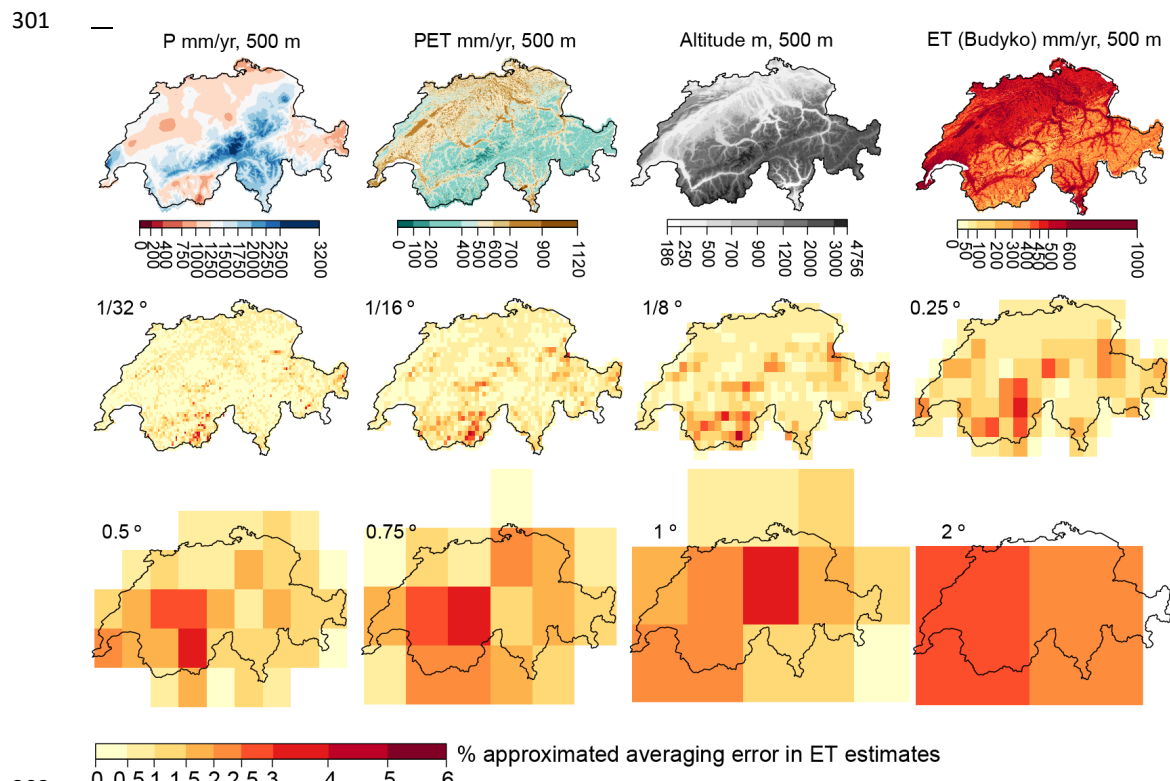
279
280 Figure 4. Estimated averaging bias (Eq. 3) across contiguous US using one-kilometer values of a) Prism P and
281 WorldClim PET c) Prism P and MODIS PET d) WorldClim P and WorldClim PET, and e) WorldClim P and MODIS PET as
282 inputs. The distribution of P and PET in the four datasets is shown in b).
283
284



285
286 Figure 5. Köppen-Geiger climate classification (Peel et al., 2007 in Beck et al. 2013) across contiguous US and the
287 distribution of corresponding calculated averaging bias in ET estimates (Eq. 3) at 1° by 1° grid cell at individual
288 climate zone shown by boxplot. The background color code in the box plot corresponds to the climate zones on the
289 left. Three data points with heterogeneity biases of over 20% are off-scale.

290
291 One may expect that future increases in computing power will lead to ESMs with smaller grid cells than those in
292 common usage today. It is therefore useful to ask how changes in ESM grid resolution are likely to affect the
293 heterogeneity biases that we have estimated in this paper. To quantify the heterogeneity bias in ET estimates as a
294 function of grid scale, we repeated our analysis at various grid resolutions using Switzerland as a test case. We
295 started with high-resolution (500m) maps of long-term average annual precipitation and PET across the Swiss
296 landscape (Fig. 6), and then used Eq. 3 to estimate the heterogeneity bias at grid scales ranging from 1/32° to 2° (~3
297 km to ~200 km). As Fig. 6 shows, aggregating P and PET over larger scales leads to larger, and more widespread,
298 overestimates in ET. Conversely, at finer grid resolutions, the average heterogeneity bias is smaller, and the
299 locations with large biases are more localized.

300



303 Figure 6. Heterogeneity bias in ET estimates at various scales across Switzerland, estimated from 500m climate
304 data. ET is calculated using the Budyko relationship (Eq. 1). Heterogeneity bias was estimated from 500m
305 precipitation (P) and potential evapotranspiration (PET), and their variances at each grid scale, using Eq. 3. At finer
306 grid resolutions, the heterogeneity bias is more localized, and smaller on average.



309 **5. Summary and discussion**

310 Because evapotranspiration (ET) processes are inherently bounded by water and energy constraints, over the long
311 term, ET is always a nonlinear function of available water and PET, whether this function is expressed as a Budyko
312 curve or another ET model. These nonlinearities imply that spatial heterogeneity will not simply average out in
313 predictions of land surface water and energy fluxes in ESMs. Overlooking the spatial heterogeneity in large scale
314 ESMs could lead to biases in estimated water and energy fluxes (e.g. ET rates). Here we have shown that, across
315 several scales, averaging over spatially heterogeneous land surface properties and processes leads to biases in
316 evapotranspiration estimates. These biases can be estimated, and these estimates can potentially be used as
317 correction factors to improve calculations of surface-atmosphere water and energy fluxes across landscapes.

318

319 In this study, we used Budyko curves as simple models of ET, in which long-term average ET rates are functionally
320 related to long-term averages of P and PET. We used an approach outlined by Rouholahnejad Freund and Kirchner
321 (2017) to estimate the heterogeneity bias in modeled ET at 1-degree grid scale across the globe (Fig. 3), and also at
322 multiple grid scales across Switzerland (Fig. 6), using finer-resolution P and PET values as drivers of ET. We showed
323 how the heterogeneity effects on ET estimates vary with the nonlinearity in the governing equations and with the
324 variability in land surface properties. Our analysis shows that heterogeneity effects on ET fluxes matter the most in
325 areas with sharp gradients in the aridity index, which are in turn controlled by topographic gradients, and not
326 merely in areas that are either arid or humid (e.g., compare Fig. 3e with Fig. 2c).

327

328 According to our analysis, regions within the U.S. that have temperate climates and dry summers exhibit greater
329 heterogeneity bias in ET estimates (Fig. 5). We show that the heterogeneity bias in ET estimates at each grid scale
330 depends on the variance in the drivers of ET at that scale (Fig. 4), and on the choice of data sources used to
331 estimate ET. Heterogeneity bias was significantly larger across the contiguous United States when P and PET data
332 sources with larger variances were used (Fig. 4).

333

334 We also explored the magnitude and spatial distribution of heterogeneity bias in ET estimates as a function of the
335 scale at which the climatic drivers of ET are averaged. We found that as heterogeneous climatic variables are
336 aggregated to larger scales, the heterogeneity biases in ET estimates become greater on average, and extend over
337 larger areas (Fig. 6). At smaller grid scales, the heterogeneity bias does not completely disappear, but instead
338 becomes more localized around areas with sharp topographic gradients. Finding an effective scale at which one can
339 average over the heterogeneity of land surface properties and processes has been a longstanding problem in Earth
340 science. Our analysis shows that at smaller resolutions the average heterogeneity bias as seen from the
341 atmosphere becomes smaller, but there is no characteristic scale at which it vanishes entirely (Fig. 6). The
342 magnitude and spatial distribution of this bias depend strongly on the scale of the averaging and degree of the
343 nonlinearity in the underlying processes. The averaging bias concept is general and extendable to any convex or



344 concave function (Rouholahnejad Freund and Kirchner 2017), meaning that in any nonlinear process, averaging
345 over spatial and temporal heterogeneity can potentially lead to bias.
346
347 One should keep in mind that the true mechanistic equations that determine point-scale ET as a function of point-
348 scale water availability and PET (if such data were available) may be much more nonlinear than Budyko's empirical
349 curves, because these curves already average over the spatial heterogeneities across spatial and temporal scales.
350 Thus, we expect that the real-world effects of sub-grid heterogeneity are probably larger than those we have
351 estimated in Sects. 3 and 4 of this study. In addition, the 1km P and PET values that are used in our global analysis
352 might be still too coarse to represent small-scale heterogeneity that is important to evapotranspiration processes.
353
354 Budyko curves are empirical relationships that functionally relate evaporation processes to the supply of water and
355 energy under steady-state conditions in closed catchments with no changes in storage. Our analysis likewise
356 assumes no changes in storage, nor any lateral transfer between the model grid cells, although both lateral
357 transfers and changes in storage may be important, both in the real world and in models. Unlike the Budyko
358 framework, ET fluxes in most ESMs are often physically based (not merely functions of P and PET) and are
359 calculated at much smaller time steps (seconds to minutes). These models often represent more processes that are
360 important to evapotranspiration (such as storage variations and lateral transfers) and include their dynamics to the
361 extent that is computationally feasible. Because these relationships may be much more nonlinear than Budyko
362 curves, there may also be significant averaging biases when complex physically based models are used to estimate
363 ET from spatially aggregated data. Therefore, we are now working to quantify aggregation bias in ET fluxes using a
364 more mechanistic land surface model.
365
366 Our results have further implications for representing sub-grid heterogeneity in hydrological parameterizations of
367 large scale ESMs, for example as sets of correction factors. However, the estimated bias shown in this study is for
368 long-term average ET estimates using a conceptual model that uses long-term annual averages. Average ET could
369 be substantially affected by temporal heterogeneity in water and energy fluxes, particularly in climates with strong
370 seasonality and shifts between water-limited and energy-limited conditions. The temporal variations in the drivers
371 of ET fluxes have not been addressed in the current study but can potentially be a source of bias for ET flux
372 estimates. Estimating aggregation bias in ET fluxes at time scales that are relevant to ESMs is therefore needed.
373 Once such bias estimations are quantified at daily or sub-daily time scales, they can be used as correction factors to
374 account for the aggregation bias in ET flux estimates.
375
376 **Acknowledgements**
377 E.R.F. acknowledges support from the Swiss National Science Foundation (SNSF) under Grant No. P2EZP2_162279.
378 The authors thank Massimiliano Zappa of the Swiss Federal Research Institute WSL for providing the 500m
379 resolution data that enabled the analysis shown in Fig. 6.



380

381 **References**

382 Aminzadeh M., and D. Or: The complementary relationship between actual and potential evaporation for spatially
383 heterogeneous surfaces, *Water Resour. Res.*, 53, 580–601, doi:10.1002/2016WR019759, 2017.

384 Avissar, R., R. A. Pielke: A Parameterization of Heterogeneous Land Surfaces for Atmospheric Numerical Models and
385 Its Impact on Regional Meteorology, *Monthly Weather Review*, vol. 117, issue 10, p. 2113, doi:10.1175/1520-
386 0493(1989)117<2113:APOLHS>2.0.CO;2, 1989.

387 Baker I. T. , P. J. Sellers , A. S. Denning, I. Medina , P. Kraus, K. D. Haynes , and S. C. Biraud: Closing the scale gap
388 between land surface parameterizations and GCMs with a new scheme, SiB3-Bins, *Journal of Advances in Modeling
389 Earth Systems, J. Adv. Model. Earth Syst.*, 9, 691–711, doi:10.1002/2016MS000764, 2017.

390 Bastiaanssen, W. G. M., M. Menenti, R. A. Feddes, and A. A. M. Holtslag: A remote sensing surface energy balance
391 algorithm for land (SEBAL): 1. Formulation, *Journal of Hydrology*, 212–213, 198–212, 1998.

392 Beck H. E., A. I. J. M. van Dijk, D. G. Miralles, R. A. M. de Jeu, L. A. Bruijnzeel, T. R. McVicar, and J. Schellekens:
393 Global patterns in base flow index and recession based on streamflow observations from 3394 catchments, *Water
394 Resour. Res.*, 49, 7843–7863, doi:10.1002/2013WR013918, 2013.

395 Boone, A., and O. J. Wetzel: A simple scheme for modeling sub-grid soil texture variability for use in an atmospheric
396 climate model. *Journal of the Meteorological Society of Japan*, 77(1), 317–333, 1998.

397 Budyko, M. I.: *Climate and life*, Academic, New York, 1974.

398 Clark, M. P., Y. Fan, D. M. Lawrence, J. C. Adam, D. Bolster, D. J. Gochis, R. P. Hooper, M. Kumar, L. R. Leung, D. S.
399 Mackay, R. M. Maxwell, C. Shen, S. C. Swenson, and X. Zeng: Improving the representation of hydrologic processes
400 in Earth System Models, *Water Resour. Res.*, 51, 5929–5956, doi:10.1002/2015WR017096, 2015.

401 Ershadi A., M. F. McCabe, J. P. Evans, J. P. Walker: Effects of spatial aggregation on the multi-scale estimation of
402 evapotranspiration, *Remote Sensing of Environment* 131, 51–62, <http://dx.doi.org/10.1016/j.rse.2012.12.007>,
403 2013.

404 Fan, Y., M. Clark, D. M. Lawrence, S. Swenson, L. E. Band, S. L. Brantley, P. D. Brooks, W. E. Dietrich, A. Flores, G.
405 Grant, J. W. Kirchner, D. S. Mackay, J. J. McDonnell, P. C. D. Milly, P. L. Sullivan, C. Tague, H. Ajami, N. Chaney, A.
406 Hartmann, P. Hazenberg, J. McNamara, J. Pelletier, J. Perket, E. Rouholahnejad-Freund, T. Wagener, X. Zeng, E.
407 Beighley, J. Buzan, M. Huang, B. Livneh, B. P. Mohanty, B. Nijssen, M. Safeeq, C. Shen, W. van Verseveld, J. Volk, D.
408 Yamazaki: Hillslope hydrology in global change research and Earth system modeling, *Water Resources Research*, 55,
409 doi:10.1029/2018WR023903, 2019.



410 Giorgi, F., and R. Avissar: Representation of heterogeneity effects in Earth system modeling: Experience from land
411 surface modeling, *Rev. Geophys.*, 35, 413–437, doi:10.1029/97RG01754, 1997.

412 Hijmans, R. J., S. E. Cameron, J. L. Parra, P. G. Jones, and A. Jarvis: Very high resolution interpolated climate surfaces
413 for global land areas, *Int. J. Climatol.*, 25, 1965–1978, doi:10.1002/joc.1276, 2005.

414 Holland, S., J. L. Heitman, A. Howard, T. J. Sauer, W. Giese, A. Ben-Gal, N. Agam, D. Kool, and J. Havlin: Micro Bowen
415 ratio system for measuring evapotranspiration in a vineyard interrow, *Agric. For. Meteorol.*, 177, 93–100, 2013.

416 Hong, S. H., J. M. H. Hendrickx, and B. Borchers: Up-scaling of SEBAL derived evapotranspiration maps from Landsat
417 (30 m) to MODIS (250 m) scale, *Journal of Hydrology*, 370, 122–138, 2009.

418 Jarvis, A., Reuter, H. I., Nelson, A., and Guevara, E.: Hole-filled SRTM for the globe Version 4, available from the
419 CGIARCSI SRTM 90m Database, <http://srtm.csi.cgiar.org> (last access: 26 February 2016), 2008.

420 Kalma, J. D., T. R. McVicar, and M. F. McCabe: Estimating land surface evaporation: A review of methods using
421 remotely sensed surface temperature data, *Surv. Geophys.*, 29, 421–469, doi:10.1007/s10712-008-9037-z, 2008.

422 Kollet S. J.: Influence of soil heterogeneity on evapotranspiration under shallow water table conditions: transient,
423 stochastic simulations, *Environmental Research Letters*, 4, 35007, doi:10.1088/1748-9326/4/3/035007, 2009.

424 Koster R. D. et al.: GLACE: The Global Land–Atmosphere Coupling Experiment. Part I: Overview. *J. Hydrometeor.*, 7,
425 590–610, 2006.

426 Koster R. D., and M. Suarez: Modeling the land surface boundary in climate models as a composite of independent
427 vegetation stands, *J. Geophysical Research*, 97 (D3), 26-97-2715, 1992.

428 Lu, H., T., Liu, Y. Yang, D. Yao: A hybrid dual-Source model of estimating evapotranspiration over different
429 ecosystems and implications for satellite-based approaches, *Remote Sens.* 6, 8359–8386, 2014.

430 Maayar, M. E., J. M. Chen: Spatial scaling of evapotranspiration as affected by heterogeneities in vegetation,
431 topography, and soil texture, *Remote Sensing of Environment*, 102, 33–51, 2006.

432 Mahrt, L., J. Sun, D. Vickers, J. I. MacPherson, J. R. Perderson, and R. L. Desjardins: Observations of fluxes and inland
433 breezes over a heterogeneous surface, *J. Atmos. Sci.* 51, 2165e2178, 1992.

434 McCabe M., and E. Wood: Scale influences on the remote estimation of evapotranspiration using multiple satellite
435 sensors, *Remote Sensing of Environment* 105 (2006) 271–285, 2006.

436 Mezentsev, V. S.: More on the calculation of average total evaporation, *Meteorol. Gidrol.*, 5, 24–26, 1955.

437 Mu, Q., F. A. Heinsch, M. Zhao, and S. W. Running: Development of a global evapotranspiration algorithm based on
438 MODIS and global meteorology data, *Remote Sens. Environ.*, 111, 519–536, doi:10.1016/j.rse.2007.04.015, (2007).



439 Peel, M. C., B. L. Finlayson, and T. A. McMahon: Updated world map of the Köppen-Geiger climate classification,
440 Hydrol. Earth Syst. Sci., 11, 1633-1644, <https://doi.org/10.5194/hess-11-1633-2007>, 2007.

441 PRISM Climate Group, Oregon State University, <http://prism.oregonstate.edu>, created 22 Feb 2017.

442 Rouholahnejad Freund, E., and J. W. Kirchner: A Budyko framework for estimating how spatial heterogeneity and
443 lateral moisture redistribution affect average evapotranspiration rates as seen from the atmosphere, *Hydrology*
444 and Earth System Sciences, 21(1), 217-233, 2017.

445 Santanello J. R., and C. D. Peters-Lidard: Diagnosing the Sensitivity of Local Land-Atmosphere Coupling via the Soil
446 Moisture-Boundary Layer Interaction, *J. Hydrometeorology*, 12, 766-786, doi: 10.1175/JHM-D-10-05014.1, 2011.

447 Sato N., P. J. Sellers, D. A. Randall, E. K. Schneider, J. Shukla, J. L. Kinter III, Y. T. Hou, and E. Albertazzi: Effects of
448 Implementing the Simple Biosphere Model in a General Circulation Model, *J. Atmospheric Sciences*, 46(18), 2757-
449 2782, 1989.

450 Seneviratne, S. I., T. Corti, E. L. Davin, M. Hirschi, E. B. Jaeger, I. Lehner, B. Orlowsky, and A. J. Teuling: Investigating
451 soil moisture-climate interactions in a changing climate: A review, *Earth-Science Reviews*, 99(3-4), 125-161, 2010.

452 Shahraeeni, E., and D. Or: Thermo-evaporative fluxes from heterogeneous porous surfaces resolved by infrared
453 thermography, *Water Resour. Res.*, 46, W09511, doi:10.1029/2009WR008455, 2010.

454 Su, Z.: The Surface Energy Balance System (SEBS) for estimation of turbulent heat fluxes. *Hydrology and Earth*
455 *System Sciences*, 6, 85-100, 2002.

456 Turc, L.: Le bilan d'eau des sols: relation entre la precipitations, l'évaporation et l'écoulement, *Ann. Agron. A*, 5,
457 491-569, 1954.

458 Wood, N., and P. J. Mason: The influence of static stability on the effective roughness length for momentum and
459 heat transfer, *Quart. J. Roy. Meteor. Soc.* 117, 1025e1056, 1991.